JANUARY 1985 LRP 229/83

LIMITER DESIGN AND MATERIAL TESTS IN TCA WITH ALFVEN WAVE HEATING

F. Hofmann, Ch. Hollenstein, B. Joye, A. Lietti,
J.B. Lister, S. Nowak, N.J. Peacock, A. Pochelon
and M.F. Stamp

LIMITER DESIGN AND MATERIAL TESTS IN TCA WITH ALFVEN WAVE HEATING

F. Hofmann, Ch. Hollenstein, B. Joye, A. Lietti, J.B. Lister,
S. Nowak[0], N.J. Peacock*, A. Pochelon, and M.F. Stamp*

Centre de Recherches en Physique des Plasmas
Association Euratom - Confédération Suisse
Ecole Polytechnique Fédérale de Lausanne
CH - 1007 Lausanne / Switzerland

*Culham Laboratory, Abingdon, GB

[0]University of Fribourg, Plasma Physics Department
CH - 1700 Fribourg / Switzerland

ABSTRACT

Following serious impurity problems encountered during the initial Alfvén Wave Heating experiments in TCA we have tested several new limiters with considerable resulting improvement.

Replacing the narrow steel bar limiters by wide, carefully profiled steel limiters led, surprisingly, to a much worse radiation dominated performance. Wide carbon limiters and TiC coated carbon limiters were then installed. The latter gave the lowest Z_{eff} but a peaked radiated power profile. We finally installed narrower pure carbon limiters with which the rf experiments could be advanced.

I. INTRODUCTION

The TCA tokamak [1] was built with the specific aim of studying Alfvén Wave Heating. Its main parameters are R = 0.6 m, a = 0.18 m, $B_{\phi} \leq 1.51$ T, $I_p \leq 170$ kA. The machine has been in operation since 1980, rf experiments were begun in 1981 [2] and the first heating results were obtained in 1982 [3]. Increases in both axial electron and ion temperatures have been measured, but the rf pulse (2.5 MHz) is always accompanied by an increase in the radiated power loss. This has been due to line emission by impurities, dominantly iron [4] since the walls, antennae and limiters were made of stainless steel. An increase in light impurity concentration was also observed.

The initial TCA limiters were in the form of four rectangular bars (top and bottom : 12x60 mm^2; inner and outer 20x40 mm^2) made from 304 L stainless steel. These were evidently inadequate for the power levels in TCA, judging by the edge melting observed (Fig. 1). In addition several experiments [5,6,7] had shown improved performance using low Z materials for the limiters. As a result, a programme of limiter design and material testing was started in order to improve on the plasma performance.

Fig. 2 shows a cross-section of the vacuum vessel with the position of the new limiters (Fig. 2 right) and their toroidal dimensions (left). The top and bottom limiters are cylindrical with a diameter of 5.5 cm. The outer limiter, which is not in the same poloidal plane, but 40 $^{\circ}$ away toroidally, is radially movable. The radii of curvature of the limiters in the poloidal sense, 22 cm for the top and bottom, 20 cm for the other two, are slightly larger than the minor plasma radius (18 cm). The cross-section in the toroidal direction, for the inner and outer limiters, was chosen so as to give a constant temperature increase over the whole surface as shown by TFR [5], but the surface temperature of the limiters has not yet been measured in TCA. The toroidal width, 12 cm, is sufficient to avoid any melting of the material even if the total plasma energy is deposited on the limiter.

Following these design criteria we constructed carefully profiled stainless steel limiters, graphite limiters and TiC coated graphite

limiters. In the following sections we shall discuss the effects of these different limiters.

This study differs from previous such studies not only in the heating method used, but also in that the diagnostic information is more complete, with spectroscopic and radially resolved bolometer measurements being made together for all limiters.

II. EXPERIMENTAL RESULTS

The comparison between the limiters was made under almost identical conditions, namely $B_{\emptyset}$ = 1.51 T, a = 0.18 m, q_a = 4.3 (3.3 for the narrow limiters), and with deuterium as the filling gas. The torus was regularly cleaned using overnight Taylor Discharge Cleaning in the filling gas. There was no gettering in the torus. The limiters were, in all cases, floating with respect to the torus potential. The central electron density was approximately 3×10^{13} cm^{-3} just before the rf pulse (2.5 MHz), which was switched on for 30 ms when the plasma resistance reached its lowest value. The rf power was limited in this study to about 80 kW for all cases except the narrow limiters when it reached 100 kW. For each particular limiter we present the main operating parameters in Table I. The evolution of the radiated power radial profile before and during the rf pulse is also presented. This was measured on a shot by shot basis using a scannable germanium bolometer. Thomson scattering measurements of peak electron temperature, combined with the resistive loop voltage allowed an estimate of $Z_{eff}(0)$ to be made for certain assumptions concerning the q-profile, namely $q(0) \sim 0.9$ for regular sawtooth discharges, and $q(0) \sim 1.3$ for others.

In addition to these standard diagnostics, a 1-meter normal incidence concave diffraction grating spectrometer (Rank-Hilger Model E 766) was used to make observations in the Vacuum Ultra-Violet region of the spectrum between 250 Å and 2800 Å. The data were recorded as a function of time during the tokamak pulse, using a TPB phosphor-photomultiplier combination. A platinum coated 1200 ℓ/mm grating blazed at 1500 Å was used for all measurements.

We have observed lines predominantly from the plasma edge, namely CIV, NV and OVI, as well as lines emanating from deeper within the plasma, such as OVII, FeXVIII, TiXIV and CrXVI. The relative intensities of these lines are tabulated in Table II, where the signal has been corrected for slit-width, phototube gain and MgF_2 filter (where necessary). In addition we correct for the relative grating efficiency $DE(\lambda)$ and for the reflectivity of the grating overcoat as a function of wavelength, $R(\lambda)$, taken from Samson [8]. The total grating efficiency is $GE(\lambda) = R(\lambda) \times DE(\lambda)$ and the form of these curves is shown in Fig. 3.

We discuss spectroscopic results for the three identically shaped limiters of stainless steel, pure graphite and TiC coated graphite; the measurements were made before the rf pulse and at the peak of the signal intensity during the rf pulse. The results obtained with each limiter are discussed in turn. The sequence in which they were tested was in fact : wide carbon, wide steel, TiC coated carbon and narrow carbon.

1) The original SS bar limiters

Figure 4 shows the time evolution of the radiated power profile. At 45 ms, before the rf pulse was switched on, the radiation was already very peaked on the axis and reaching 1 W/cm^3, about one half of the ohmic power. This value can only be explained by radiation due to metallic impurities [4]. The ratio of radiated to ohmic power, shown in Fig. 5, is about 0.6 before the rf pulse (140:230 kW) and greater than 1.0 with 80 kW of rf power. The increase in radiation during the heating pulse can partly be explained by the density increase which is up to 20% of the line-average density at this rf power level, but the impurity concentration also increases. This was shown by spectroscopic measurements on core iron lines, for example FeXVIII and FeXIX, the intensities of which increased by a factor of 2-3 during the pulse [4]. This high impurity concentration was the cause of a very resistive discharge with an associated loop voltage of 2.4 V during the current plateau.

2) Wide stainless steel limiters

We found, surprisingly, no improvement when replacing our bar limiters made from 304 L stainless steel by carefully profiled wide limiters made from the same steel and indeed would infer a degradation. It was in fact found to be impossible to produce sawtoothing discharges, which had been achieved with the old bar limiters after intensive cleaning. The radiated power on the axis reached a value of about 1.5 W/cm^3 in the ohmic part of the discharge (Fig. 6). Figure 5 shows that the total radiation losses corresponded to 70 % of the ohmic power and the resistive loop voltage reached 2.9 V. During the rf pulse, the huge increase in radiation at the centre again might have been partly due to the increase in density, slightly larger than in the previous case, as well as to a larger density peaking factor, but the impurity density also increased as before. The intensities of the impurity lines is tabulated in Table II. We see that there is a large increase in the edge lines intensities as well as in the central lines. The edge lines (CIV, NV, OVI) generally increase by a factor of ~ 2.1-2.7 at about 80 kW rf power. The different shape of the edge line waveforms with respect to that of the core lines, as discussed in [4] was maintained. The core lines increased by a factor of ~ 2.5-3 but did not generally reach a steady state.

Following the poor behaviour of these limiters, compared with the original ones, we suggest that the increase in the surface area of the limiters increases the sputtering yield by more than the advantage gained from lowering the operating surface temperature. Observations of the limiters after about 400 discharges did not reveal any traces of melting and only a very few points of arcing damage.

3) Carbon limiters

The graphite for the carbon limiters (5890 PT from Carbone-Lorraine, France) was machined, ultrasonically cleaned in distilled water, and then out-gassed at 1200 °C. Unfortunately, the oven used for this latter process produced a slight metallisation of the surface, and an Auger analysis showed up 6-8 % of metallic impurities (mainly iron and chromium) on the surface.

The insertion of carbon limiters led to a large reduction of both the resistive voltage (to about 2V), and the radiated power loss. The ratio P_{rad}/P_{oh} (Fig. 5) was down to 0.5 in the ohmic part of the discharge and reached 0.8 during the rf pulse. The radiation on axis (Fig. 7) did not exceed 1.1 W/cm^3. The fact that we never observed a hollow radiation profile indicated that metallic impurities remained responsible for the radiation losses at the centre. Typical discharges with these contaminated carbon limiters had a Z_{eff} value of 3.5. After about 1250 discharges the limiters were practically unchanged in appearance. We note that these limiters produced regular sawtooth-dominated discharges after very little conditioning following their insertion, presumably due to the more favourable radiated power profile. The residual gas partial pressure of methane increased by a large factor following the insertion of the graphite limiters.

The intensity of the FeXVIII line was considerably reduced, compared with the case of the wide steel limiters. The peak value, during rf, was down by a factor of 2.5, as was the pre-rf value. This corresponds reasonably with the observed reduction in the radiated power loss on axis. The intensity of the OVII line was roughly the same before the rf pulse was applied, compared with the stainless limiters, as was its increase during the rf pulse. We cannot,therefore, relate the reduction in iron content to a change in oxygen content and hence to reduced oxygen sputtering from the antennae and walls. If sputtering by oxygen is the major cause of the iron influx, then it occured mainly on the steel limiters themselves. This is in agreement with the increase in iron content with wider limiters. With the exception of the low ionization stages of carbon, which increased in intensity, the edge-line intensities were reduced.

4) TiC coated carbon limiters

After being used in TCA for about 1250 discharges, the carbon limiters were polished to remove the impurities, cleaned, out-gassed, and used as a base for the TiC coating. The 7.5-9 μm coating was deposited by Chemical Vapour Deposition by the Laboratoire Suisse de Recherche Horlogère (Neuchâtel, Switzerland) and the limiters were cleaned and out-gassed at 1000 °C, to avoid contamination.

With the TiC coated carbon limiters, the radiated power on axis was even lower (0.3 W/cm^3) before the rf pulse (Fig. 8) but increased to 1.7 W/cm^3 at the end of the 30 msec pulse. The resistive voltage was as low as 1.6 V and Z_{eff} was about 2.5. The fact that the titanium has a much higher nuclear charge than carbon is counteracted by the lower sputtering yield of the TiC coating. The significant difference between the C and TiC limiters is the relative increase in the core radiation during the rf pulse. The TiC limiters were used for some 1300 discharges and the coating was only removed on a small point on the upper part of the outer limiter, presumably due to excessive local heating by runaway electrons. The residual gas partial pressure of methane decreased by a factor of 10 compared with the pure graphite limiters, due to the negligible chemical erosion of the TiC coating.

Spectroscopic measurements (Table II) showed similar relative increases in the edge lines (CIV,NV,OVI), typically by a factor of 2-2.5, when the rf pulse was applied. We also detected the presence of titanium in the plasma. The intensity of FeXVIII, probably representative of concentration, was reduced in the ohmic phase. There was, however, a larger relative increase in the core iron lines during the rf pulse.

5) Narrow carbon limiters

The first carbon limiters were unfortunately slightly metallised. On the other hand, the stainless steel limiters had shown that a big limiter surface area favours the production of impurities by sputtering. These two reasons led us to use a new set of pure carbon limiters with a reduced toroidal width of 6 cm. The central radiation power (Fig. 9) is indeed much smaller, only 0.16 W/cm^3 before and 0.7 W/cm^3 during the rf pulse. The central ohmic heating power densities are estimated to be ~2.0, 2.8 W/cm^3 respectively. This profile was obtained with 2 conditions differing from the previous profiles, namely q_a = 3.3 and P_{rf} = 100 kW. The ratio P_{rad}/P_{oh} as shown in Fig. 5 is 0.35 before the heating. In spite of the higher current, the loop voltage, 1.7 V, was lower than the previous carbon limiter case, indicating a lower impurity content and we estimate Z_{eff} to be ~2.0.

These limiters therefore produced the optimal ohmic and rf-heated plasmas. The iron intensity was still measurable, suggesting that the walls or, more likely, the rf antennae were an additional source of iron contamination.

III. ABSOLUTE IMPURITY CONCENTRATION

We have attempted to calculate the absolute concentrations of the observed heavy impurity ions in the following way. Firstly, as described by Stamp et al. [4], we assume that the radiated power from the plasma centre is due to the metallic impurities, since the light impurities will be merely radiationless fully stripped nuclei in the core, and so :

$$P_{rad}(0) = n_e \, n_{Metal} \, P_{Metal} \; W/cm^3 .$$

The factor P_{Metal}, the radiated power per metal ion per electron per unit volume is roughly constant for our conditions and has a value 0.5×10^{-25} W/cm^3/atom/electron.

Using this assumption we now calculate the concentration of FeXVIII ions. Firstly, we assume that the iron fraction of ions contributing to the radiated power from the plasma core is similar to the fraction of iron in the stainless steel of the torus walls (and limiters when they were steel), that is to say 68 %. We calculate the abundance of the iron ions as a function of radius assuming coronal equilibrium, as shown in Fig. 10, from which its average radius $\langle r \rangle$ and its typical full half-width Δr are found to be 5.5 cm and 6 cm respectively. The emitting volume and its acceptance by the spectrometer, which viewed the plasma obliquely, were calculated for concentric flux surfaces centred on the geometric axis. The instrument aperture was effectively stopped down by the 63 mm diameter torus port. The intersection of the toroidal volume with the viewing cone was then numerically calculated, and the result is shown in Fig. 11 together with integrated volume.

The sensitivity of the instrument can now be "calibrated" and we consider the case of the wide steel limiters (see Table IV).

$$n(Fe) = \frac{P_{rad}(o) \cdot 0.68}{n_e(o) \cdot 0.5 \cdot 10^{-25}}$$

$$n(Fe) = 5.9 \cdot 10^{11} \text{ cm}^{-3}$$

We estimate that , averaging over the core,

$$n(\text{Fe XVIII})/n(\text{Fe}) \sim 0.19$$
$$\text{so } n(\text{Fe XVIII}) \sim 1.12 \times 10^{11} \text{ cm}^{-3}$$

From Lawson et al. [9] we know that

$$I(\text{FeXVIII @ 975 Å}) \sim 310 \text{ ph s}^{-1} \text{ sr}^{-1} \text{ ion}^{-1} \text{ at } n_e \simeq 3.0 \times 10^{13} \text{ cm}^{-3}$$

The photon flux at the entry slit of the instrument is therefore

$$\phi = 1.12 \cdot 10^{11} \cdot 310 \; \frac{30.000 \text{ cm}^3}{4 \cdot \pi \cdot 180^2}$$

This produces a phototube signal which leads us to the final absolute intensity calibration :

$$PM\,sig\,(corrected) = N(imp) \left(\frac{Vol}{4\pi r^2}\right) I(imp) \cdot CAL$$

$$CAL = \frac{0.18}{2.56 \cdot 10^{12}} = 7.0 \cdot 10^{-14}$$

$$N(imp) = \frac{PM\,sig\,(imp.)}{\left(Vol/4\pi r^2\right) \cdot I(imp) \cdot 7.0 \cdot 10^{-14}} \cdot \frac{1}{Fraction\ in\ state}$$

We have performed this calculation for the core lines and the results are tabulated in Table III.

We note that several sources of error occur in these calculations. Firstly, the atomic physics factors are not known extremely

precisely. Secondly, there will be some error in the assumed shape of the calibration curve (Fig. 3). Further, the calibration provides a systematic over-estimate since we have assumed coronal equilibrium. Calculations for iron by Carolan and Piotrowicz [10] have shown that under our conditions, $n_e \sim 3x10^{13}$ cm^{-3}, $\tau_p \sim$ 8-15 msec the stationary state has almost had enough time to establish itself. As a result, the real radiated power loss is only slightly greater than the coronal equilibrium would predict for a given impurity density, and the calibration is therefore only over-estimated by a factor of 1.05.

The effects of anomalous diffusion were investigated by Roberts [11]. With a diffusion coefficient of 10^4 cm^2s^{-1} for our conditions, the power radiated by the iron ions is increased by 30-40%. This leads to an over-estimated value for the iron concentration derived before. On the other hand, diffusion produces a larger radial width of the emitting shell increasing its volume and leading again to an over-estimate of the calibration factor. Since the maximum abundance temperatures of the observed lines vary considerably, the effects of radial diffusion will produce differing correction factors for each line.

All these effects lead to a large error bar in the case of the metal ions iron, titanium and chromium. The calculated ratio between chromium and iron densities (0.66-2.0) is not equal to the ratio in the bulk stainless steel (0.28), as explicitly assumed in the "calibration". In the case of the TiC limiters the considerable reduction in iron and chromium densities is accompanied by a large increase in the titanium density.

The calculated oxygen density represents typically about 10 % of the electron density. This density, together with the calculated metal density, would yield a Z_{eff} of greater than 10, in disagreement with the value of ~6 estimated on axis from the electron temperature, loop voltage and assumed value of safety factor ($q_0 \sim 1.3$) in the case of the wide steel limiters. Two effects can lead to errors in this calculation. Firstly the effect of inward diffusion, modelled in detail by Roberts [11], leads to an inward shift of the OVII radius and, most importantly, a large increase in the width over which OVII is the dominant emitting state. A factor of 5 increase in the emitting volume

was obtained in that study by increasing the effective inward diffusion coefficient from 0 to 10^4 cm^2/s. The total number of impurity ions nonetheless has remained the same. Secondly a recent study by Tendler et al. [12] has shown the importance of the resonant hydrogen-oxygen charge-exchange cross-section. This has the effect of reducing the charge state to below its equilibrium value which in turn has been shown to move the emitting shell. All these effects must be taken into account to calculate correctly the oxygen density from a single chordal observation. Attempts were made to interpret the OVI signal strength and the discrepancy was found to be even greater than in the case of OVII. This is to be expected, because OVI is an edge-line, and cannot be said to be in coronal equilibrium. Recombination is probably unimportant so it is more likely to be dependent upon the OVI impurity influx. Edge-lines are not to be trusted to give a measure of impurity concentration. As a result of all these uncertainties, the estimates of absolute impurity densities must be considered to possess large error bars, especially for low Z elements.

IV. INTERPRETATION OF THE BOLOMETRIC MEASUREMENTS

In this section, we describe a simulation based on the assumption of coronal equilibrium and using the results of the calculation by Post et al. [13], as well as the measured profiles of electron density and temperature, and radiated power. We assume that iron is the only heavy impurity, since the walls and antennae made of SS 304 L contain about 68 % iron, the rest being mainly chromium and nickel which have very similar radiation properties, and that oxygen is representative of the dominant light impurities.

As in the preceeding section, the values of radiated power and electron density at the centre allow us to calculate the metallic ion concentration neglecting the very small contribution of light impurities to the radiation on axis. We next determine the oxygen concentration on axis so as to get, together with the iron content, the measured value of $Z_{eff}(0)$ by assuming that $q = 0.9$ when the soft X-ray signal showed strong sawtooth activity. This way of deriving a light impurity concentration is much less sensitive to the model used than

the line-radiation measurements. Then we choose the impurity peaking factor to get a radiation profile as close as possible to the measured one. This also permits us to calculate $Z_{eff}(r)$, $q(r)$ and obviously I_p, and to compare these values with the measured ones.

In this way we have simulated the radiation profile for the case of the greatest radiative power loss (Fig. 6 wide steel limiters) and best case (Fig. 9 narrow carbon limiters) at two differents times, just before the rf pulse and at the moment of maximum radiation on axis. Fig. 12 shows as an example the profiles of radiated power, both measured and simulated, and of Z_{eff} for the carbon limiters with 100 kW of rf heating power. The agreement between the two curves is surprisingly good for a calculation at coronal equilibrium and without diffusion terms. The results for the two cases are summarized in Table IV. The change from wide steel to carbon limiters has reduced the Z_{eff} by more than a factor of two, both during the ohmic phase and with rf heating. The heavy ion concentration decreased by a factor of 6-8 indicating that most of the heavy impurities come from the limiters. The light impurity concentration is about the same for all the limiters, in agreement with the spectroscopic measurements.

One important remark is that the peaking factor of metallic ions for the SS case is always greater than the peaking factor of electron density, suggesting an accumulation of these ions in the core of the discharge even without rf power. This is no longer the case with the carbon limiters for which a constant impurity concentration profile (heavy and light) explains the measurements quite well. From these results, we cannot conclude that there is a stronger accumulation of impurities at the centre during the rf pulse.

V. CARBONISATION OF THE WALLS

We found that use of the bare graphite limiter led to a significant and visible deposit on the torus walls. This deposit had the appearance of a treacle-coloured layer, of irregular thickness and

covered mainly the inner vertical walls, but also the observation windows. This layer was sufficiently thick after several months of operation to be peeled away from the inner wall.

The deposition is considered to be a result of either the prolonged Taylor Discharge Cleaning used in TCA or the tokamak discharges themselves. The TDC takes the form of 30 msec pulses at 5 kHz, at a repetition rate of 2 Hz, and is run each night, and all weekend. Thus we run up a total of ~0.7 hour of TDC plasma duration each night, and 3.6 hours of TDC plasma duration at the weekend. It is possible that methane production may be significant during TDC (as it is found to be after a tokamak shot) and we assume that the cracking of the methane either during TDC or during the shots led to the carbonisation of the wall.

Unfortunately, this may confuse the interpretation of the effects of the limiter changes, since the carbonisation will have reduced the production of iron from the walls, and possibly from the antennae, although the latter did not have a visible coating, possibly due to their increased temperature during TDC, being immersed in the plasma.

VI. TOROIDAL ROTATION MEASUREMENTS

A final part of the spectroscopic study was a measurement of relative toroidal velocity of the plasma impurity ions in view of its possible relation with impurity transport. For this work the spectra were recorded on 101-01 photographic film and digitised. The spectrometer viewed the plasma almost tangentially, so that any plasma motion could be detected as Doppler shifts in the spectral lines emitted by the plasma. The dispertion curve $dl/d\lambda$ ($cm\AA^{-1}$) was evaluated using the known wavelengths of low ionization state peripheral ions as fiducials to which a polynomial was fitted. The other available lines were then measured and a relative wavelength shift was calculated and interpreted as a relative Doppler shift. The radius of maximum emittance

for a given line was taken as the radius corresponding to the temperature of maximum abundance. Thus to each line could be ascribed a radius. The plot of relative wavelength shift against this radius is shown in Fig. 13 both with and without rf. We observe that there is a small, consistent blue shift towards the plasma centre. This corresponds to ion velocities "faster" parallel to the electron drift in the centre, or, obviously, "faster" against the electron drift at the plasma edge. The results with and without rf are essentially identical within the error bars of these preliminary measurements (about 1×10^6 cm/sec). We cannot therefore claim to measure a significant change in toroidal rotation during the rf pulse.

VII. CONCLUSION

By changing the design and material of the limiters in TCA we have reduced the heavy impurity concentration by a factor of about 6, and the ratio of radiated to ohmic power on axis by more than 3. We are still using the narrow carbon limiters which gave the smallest absolute radiated power loss. Surprisingly, the operation of the machine with the low power density wide steel limiters was more difficult than with the bar limiters, suggesting that greater sputtering of the larger area limiters plays an important role in impurity production. The surface area may, in fact, be so large that the Taylor Cleaning and tokamak discharges never remove the loosely bonded oxygen from the surface. Although the TiC limiters were much appreciated for ohmic discharges, they led to a relatively large radiated power loss at the centre during the rf pulse.

The fact that we have not yet observed a genuinely hollow radiated power profile is probably explained by the heavy impurities coming from the antennae and perhaps the walls.

ACKNOWLEDGEMENTS

The collaboration of the whole TCA team is acknowledged in this work, which was partly financed by the Swiss National Science Foundation.

REFERENCES

[1] A.D. Cheetham et al., Proc. 11th Symp. Fusion Technology (1980), Oxford, Pergamon Press 1981, vol. 1, p. 601

[2] A. de Chambrier et al., Plasma Physics 24 (1982) 893

[3] A. de Chambrier et al., Plasma Physics 25 (1983) 1021

[4] M.F. Stamp, A. Pochelon, N.J. Peacock, J.B. Lister, B. Joye and H. Gordon, Lausanne Report LRP 220/83 (1983)

[5] Equipe TFR, Journal of Nuclear Materials, 105 (1982) 62

[6] Y. Gomay et al., Journal of Nuclear Materials, 111 + 112 (1982) 323

[7] L.C. Emerson et al., Journal of Nuclear Materials, 103 + 104 (1981) 199

[8] J.A.R. Samson, "Techniques of VUV spectroscopy", Wiley, 1967

[9] J.D. Lawson, N.J. Peacock and M.F. Stamp, J. Phys. B14 (1981) 1929 - 1952

[10] P.G. Carolan, V.A. Piotrowicz, Plasma Physics 25 (1983) 1065

[11] D.E. Roberts, Nuclear Fusion 21 (1981) 215

[12] M. Tendler, J. Neuhauser, R. Wunderlich, IPP-Report, IPP I/221 (1983)

[13] D.E. Post, R.V. Jensen, C.B. Tarter, W.H. Grasberger, W.A. Lokke, Atomic Data and Nuclear Data Tables 20, 5 (1977) 397

FIGURE CAPTIONS

1. Stainless-Steel bar limiter melting.

2. Design of the limiters.

3. Correction factors for estimating line intensities.

4. Evolution of the radiated power profile : original bar limiters.

5. Ratio of P_{rad}/P_{oh} in various conditions. (Start of rf-pulse aligned).

6. Evolution of the radiated power profile : wide stainless steel limiters.

7. Evolution of the radiated power profile : wide carbon limiters.

8. Evolution of the radiated power profile : TiC coated carbon limiters.

9. Evolution of the radiated power profile : narrow carbon limiters.

10. Radial profile of iron states.

11. Effective viewed volume as a function of minor radius (quasi-tangential viewing).

12. Radiated power profiles and calculated radial profile of $Z_{eff}(r)$ for the carbon limiters with 100 kW of rf power.

13. Relative toroidal velocity as a function of minor radius, with and without rf.

LIST OF TABLES

I. Summary of different operating conditions.

II. Summary of observed line intensities.

III. Estimates of impurity concentration from spectroscopic measurements.

IV. Results of bolometric profile simulation.

TABLE I

	Bar stainless steel	Wide steel	Carbon (contaminated)	TiC	Narrow carbon (clean)
I_p(kA)	97	97	97	97	125
q_I	4.3	4.3	4.3	4.3	3.3
V_L	2.4	2.9	2.	1.6	1.7
$n_e(0)$ 10^{13} cm^{-3}	2.7	2.7	2.8	2.8	2.8
P_{oh}(kW)	240	280	194	155	227
P_{rad}(kW)	140	190	100	75	80
$P_{rad}(0)$(W/cm^3)	1.0	1.5	0.4	0.3	0.16
Z_{eff}	4.0	4.2	3.5	2.5	2.
P_{rad}/P_{oh}	58%	68%	52%	48%	35%

TABLE II

					Intensities					
Line	λ(Å)	Gain	Slits	GE(λ)	SS		C		TiC	
					Pre-rf	Peak	Pre-rf	Peak	Pre-rf	Peak
CIV	1548.2	.5	1	.53	.72	1.9	1.4	3.0	.71	1.7
NV	1238.8	.5	1	.38	.95	2.05	.90	2.05	1.1	2.5
OVI	1031.9	.5	1	.25	4.2	8.8	5.2	11.5	5.6	13.6
OVII	1623.7	8.0	3.0	.54	.086	.13	.093	.15	.10	.19
FeXVIII	974.7	8.0	3.0	.23	.18	.47	.10	.19	.06	.20
TiXIV	2117.1	8.0	3.0	.6	-	-	-	-	.014	.035
CrXVI	1410.6	8.0x.69*	3.0	.45	.047	.12	.056	.11	.009	.026

*Corrected for MgF_2 window

TABLE III

								Impurity ion density (cm^{-3})					
								SS		C		TiC	
	$\hat{T}_e$	<T> (cm)	Δr (cm)	$n(\langle r \rangle)$ (cm^{-3})	$\frac{N(state)}{N(ion)}$	Volume	I(imp)	Pre-rf	Peak	Pre-rf	Peak	Pre-rf	Peak
FeXVIII	650	5.5	6	3	0.19	30.0×10^3	310*	0.55×10^{12}	1.5×10^{12}	0.3×10^{12}	0.6×10^{12}	0.18×10^{12}	0.6×10^{12}
TiXIV	365	8.5	3	2.8	0.2	15.3×10^3	35	-	-	-	-	0.76×10^{12}	1.9×10^{12}
CrXVI	473	6.5	3	3.2	0.16	16.3×10^3	126+	0.65×10^{12}	1.7×10^{12}	$.75 \times 10^{12}$	1.5×10^{12}	0.12×10^{12}	$.36 \times 10^{12}$
OVII	178	11.6	2.6	2.1	1.0	14.1×10^3	13.5*	2.6×10^{12}	4×10^{12}	2.8×10^{12}	4.6×10^{12}	3.0×10^{12}	5.8×10^{12}

* Lawson et al. (1981)

+Gordon (1983)

TABLE IV

		SS		C-2	
		40 ms	60 ms	70 ms	100 ms
$n_e(0)$		2.7×10^{13}	35×10^{13}	2.8×10^{13}	3.9×10^{13}
κ_n		1	1.8	1.25	1.4
V_R		2.9	3.6	1.7	2.4
I_p(kA)		97	80	125	120
$P_{rad}(0)$ W/cm^3		1.5	3.2	0.16	0.69
$P_{oh}(0)(q_0=0.9)$		3.4	3.7	1.97	2.8
Heavy Imp.	η_M	4%	5.5%	0.5%	0.9%
	κ_M	2.5	3.5	1.25	1.4
	n_M	1.1×10^{12}	1.9×10^{12}	0.14×10^{12}	0.35×10^{12}
Light Imp.	η_L	2%	3%	1.5%	4.5%
	κ_L	1	1.8	1.25	1.4
	n_L	0.54×10^{12}	1.05×10^{12}	0.42×10^{12}	1.7×10^{12}
Z_{eff} (meas.)		4.2	6.8	1.9	3
Z_{eff} (calc.)		4.1	4.5	2.4	3.6

FIG.1

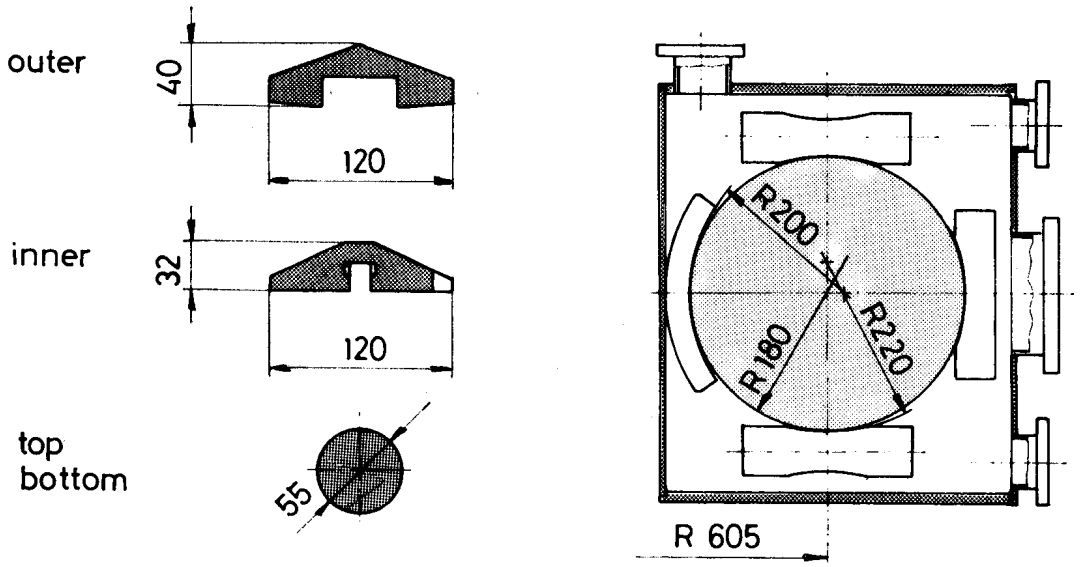

FIG.2 Design of the limiters

(dimensions in mm)

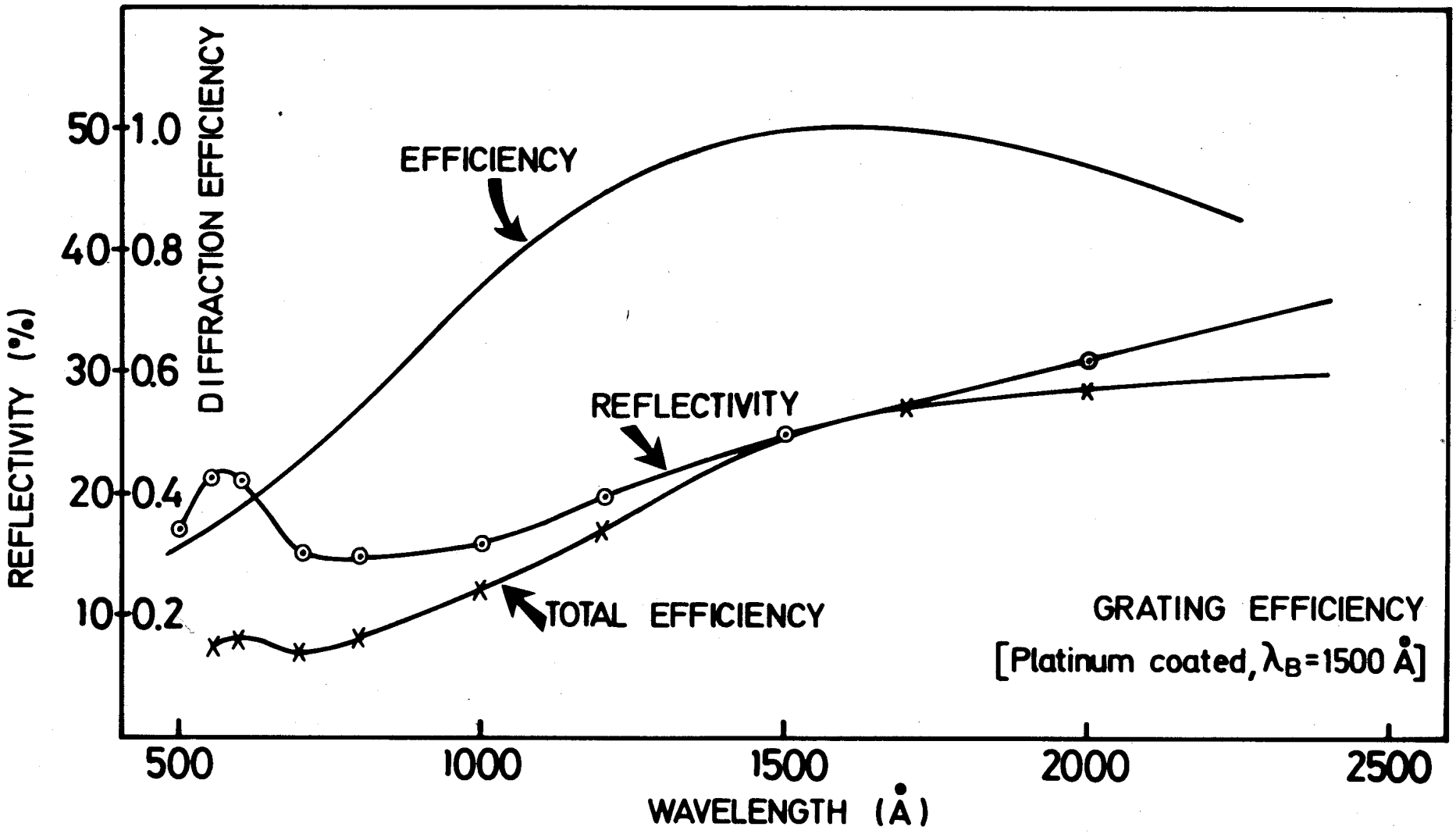
REFLECTIVITY (%)
DIFFRACTION EFFICIENCY
50
40
30
20
10
1.0
0.8
0.6
0.4
0.2
EFFICIENCY
REFLECTIVITY
TOTAL EFFICIENCY
GRATING EFFICIENCY
[Platinum coated, λ_B=1500 Å]
500
1000
1500
2000
2500
WAVELENGTH (Å)

FIG.3

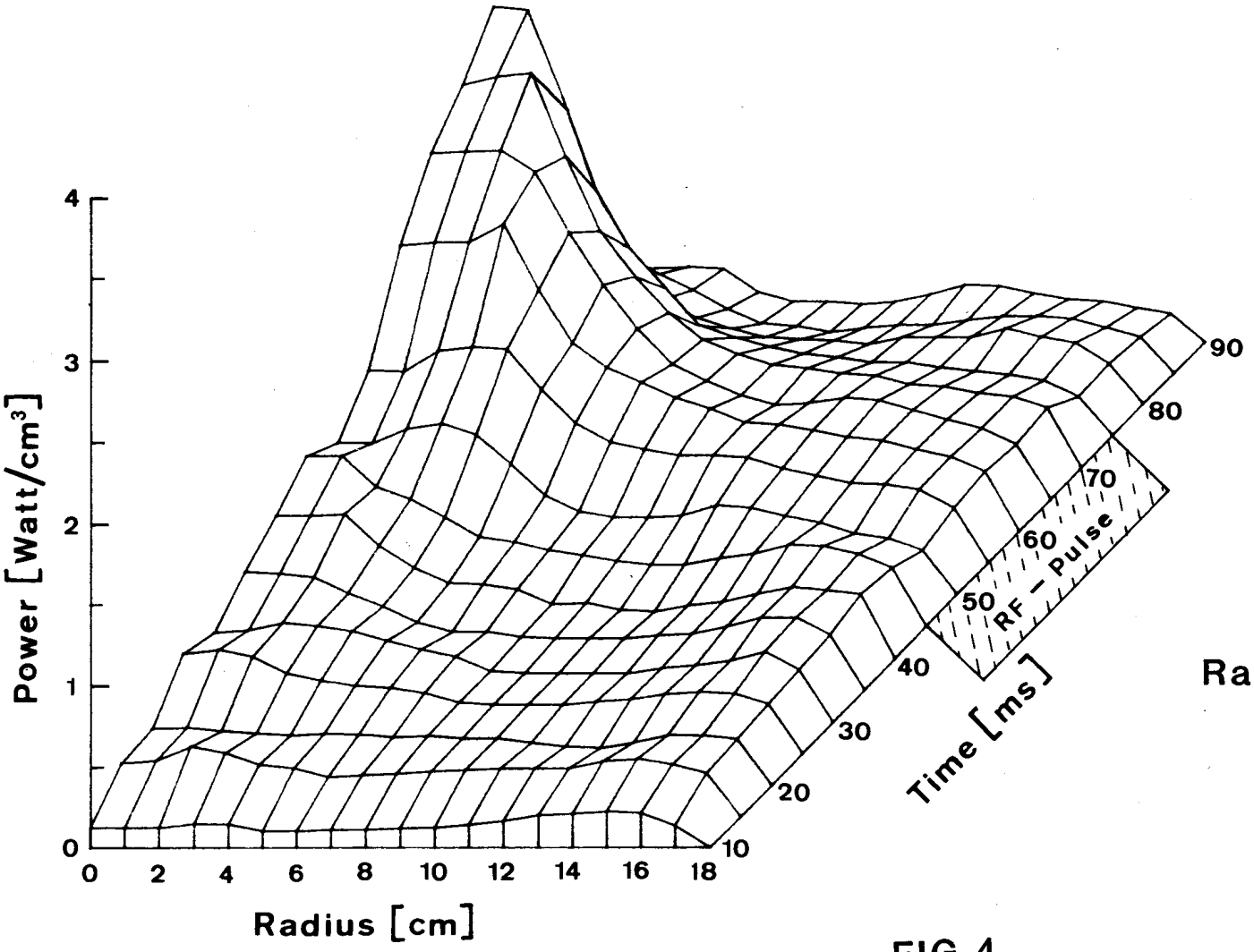

Radiated power profile

Bar SS limiters

FIG.4

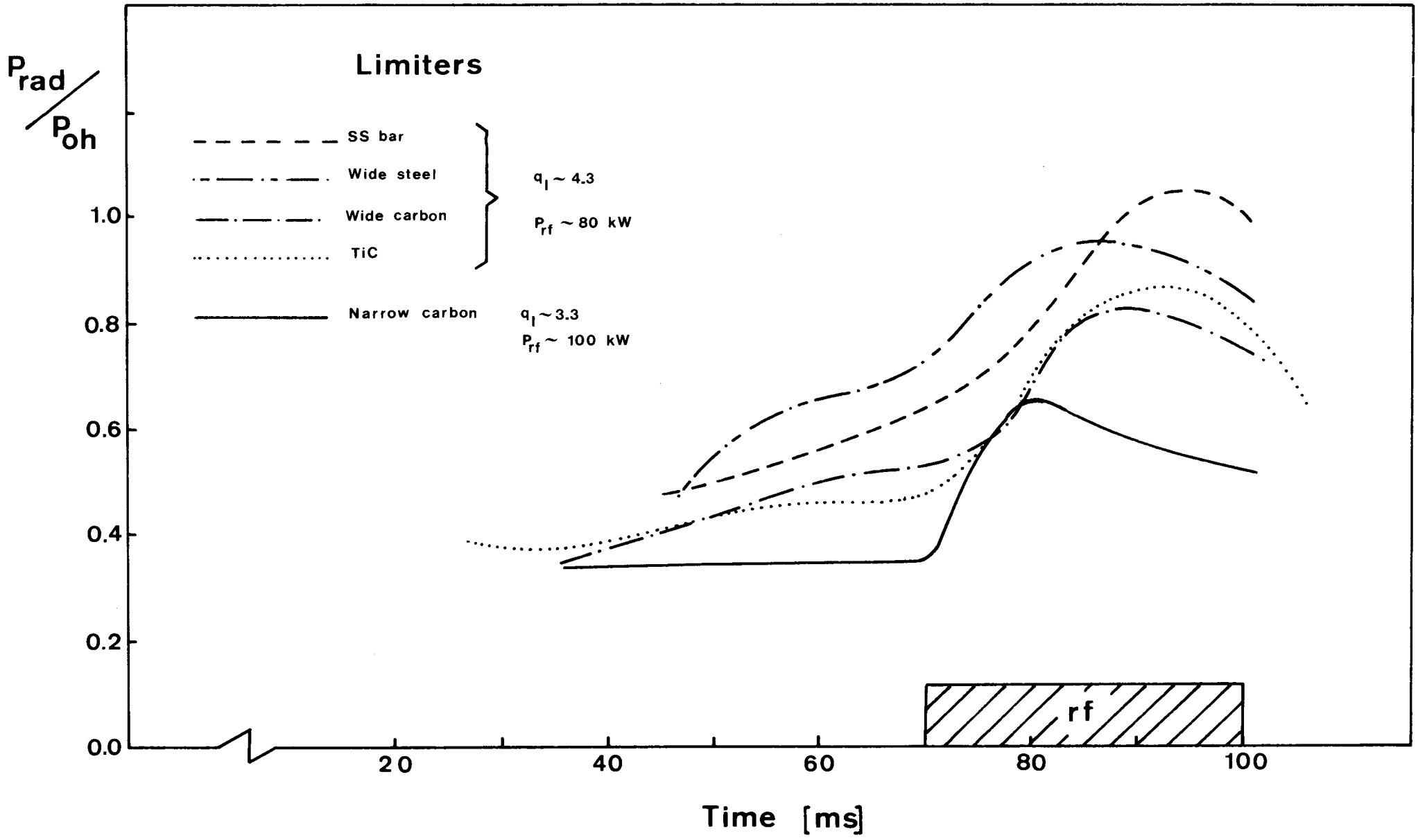
Limiters
P_{rad}/P_{oh}
SS bar
Wide steel
Wide carbon
TiC
$q_l \sim 4.3$
$P_{rf} \sim 80$ kW
Narrow carbon
$q_l \sim 3.3$
$P_{rf} \sim 100$ kW
1.0
0.8
0.6
0.4
0.2
0.0
20
40
60
80
100
rf
Time [ms]

FIG.5

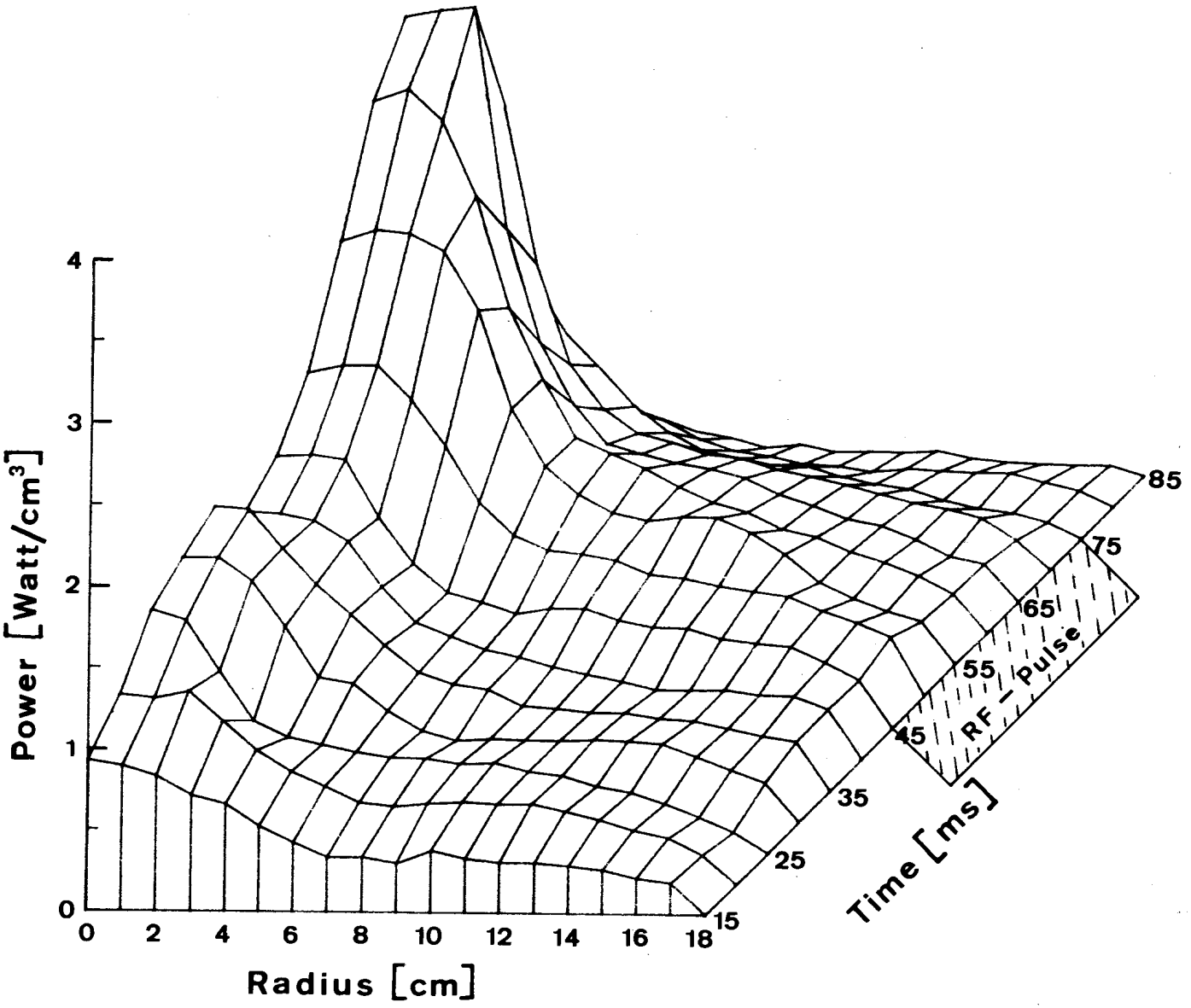

Wide steel limiters

FIG.6

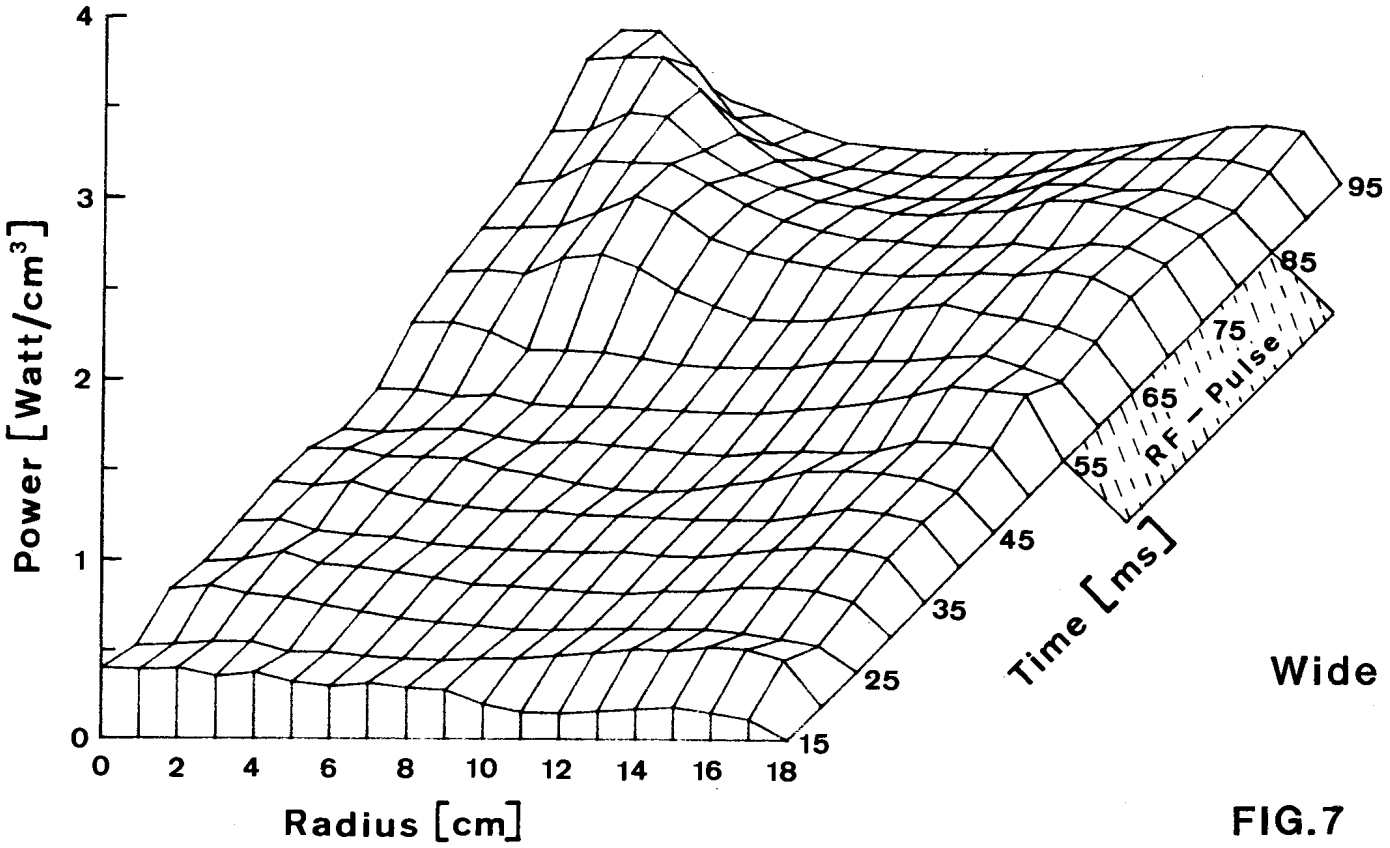

Wide carbon limiters

FIG.7

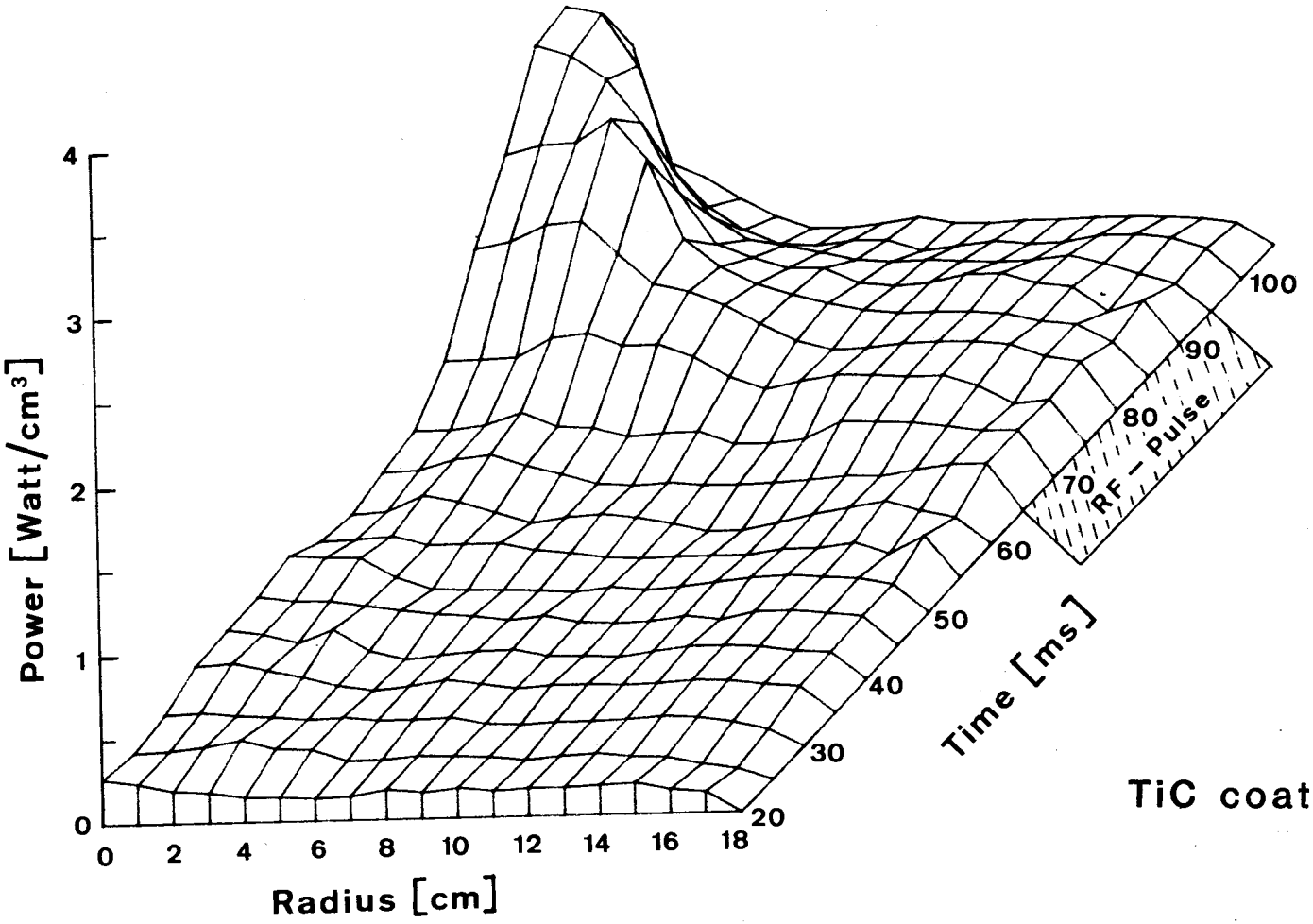

TiC coated carbon limiters

FIG.8

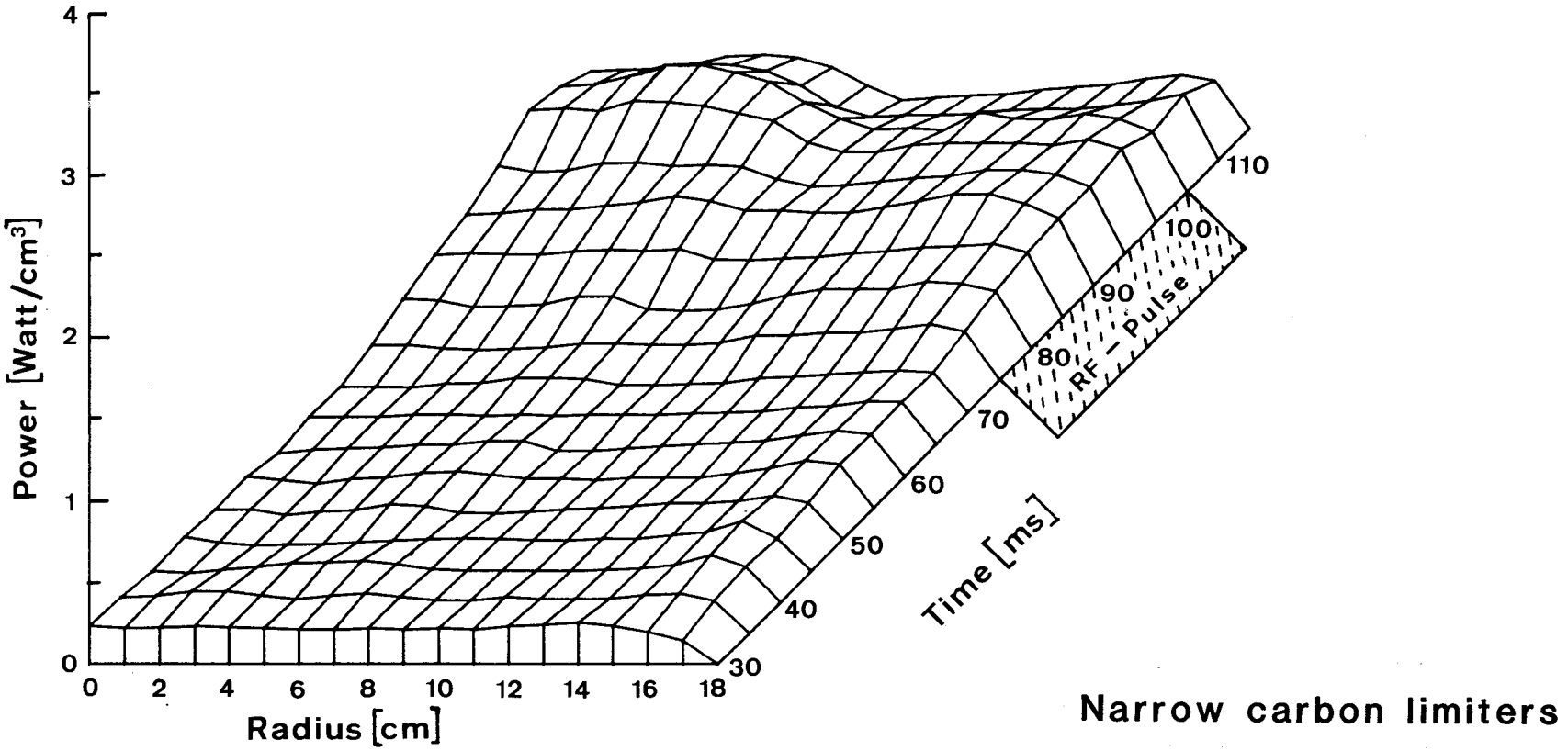
Power [Watt/cm³]
4
3
2
1
0
0
2
4
6
8
10
12
14
16
18
Radius [cm]
30
40
50
60
70
80
90
100
110
Time [ms]
RF – Pulse
Narrow carbon limiters

FIG.9

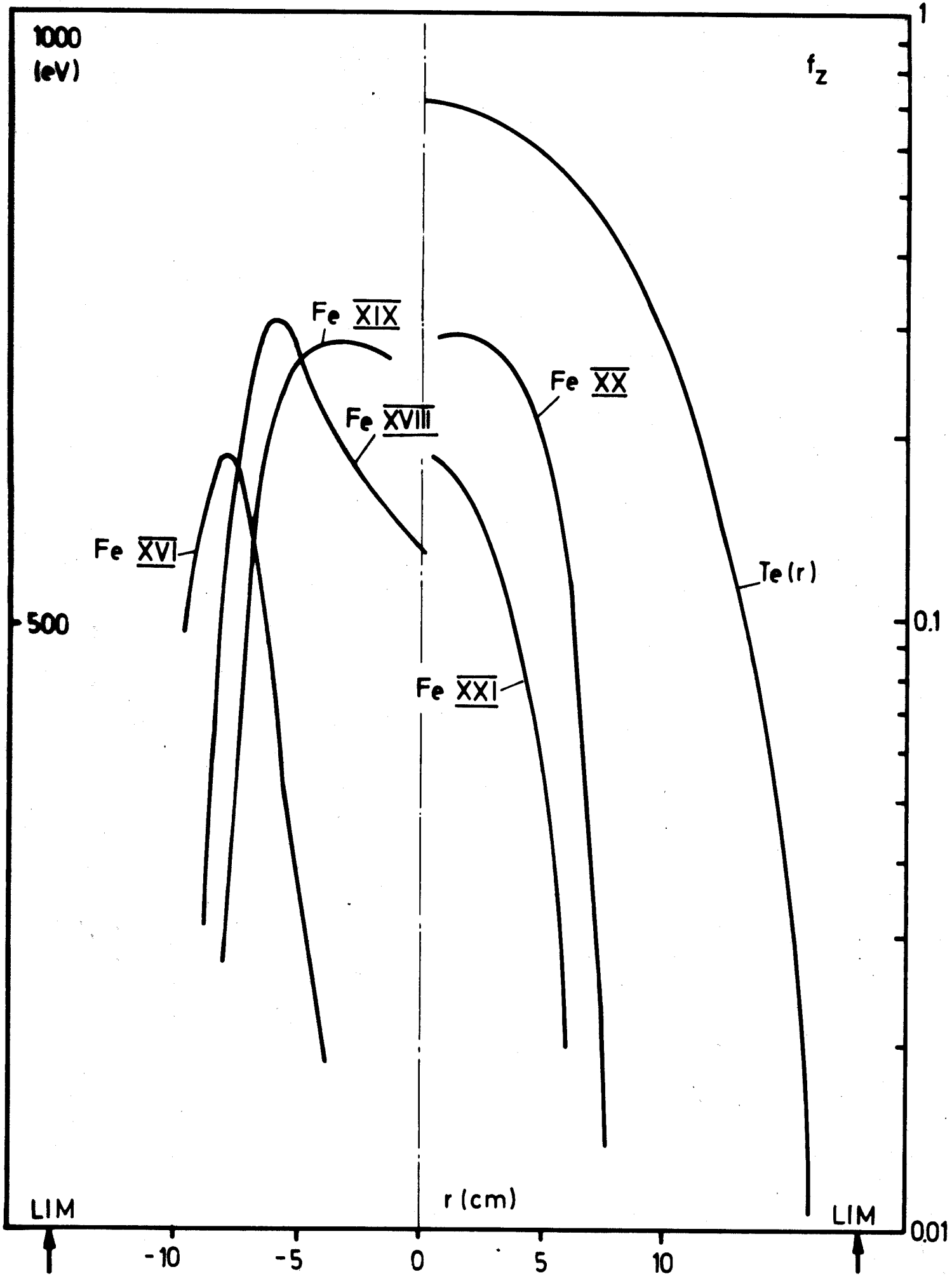

FIG. 10 **Radial profile of iron states**

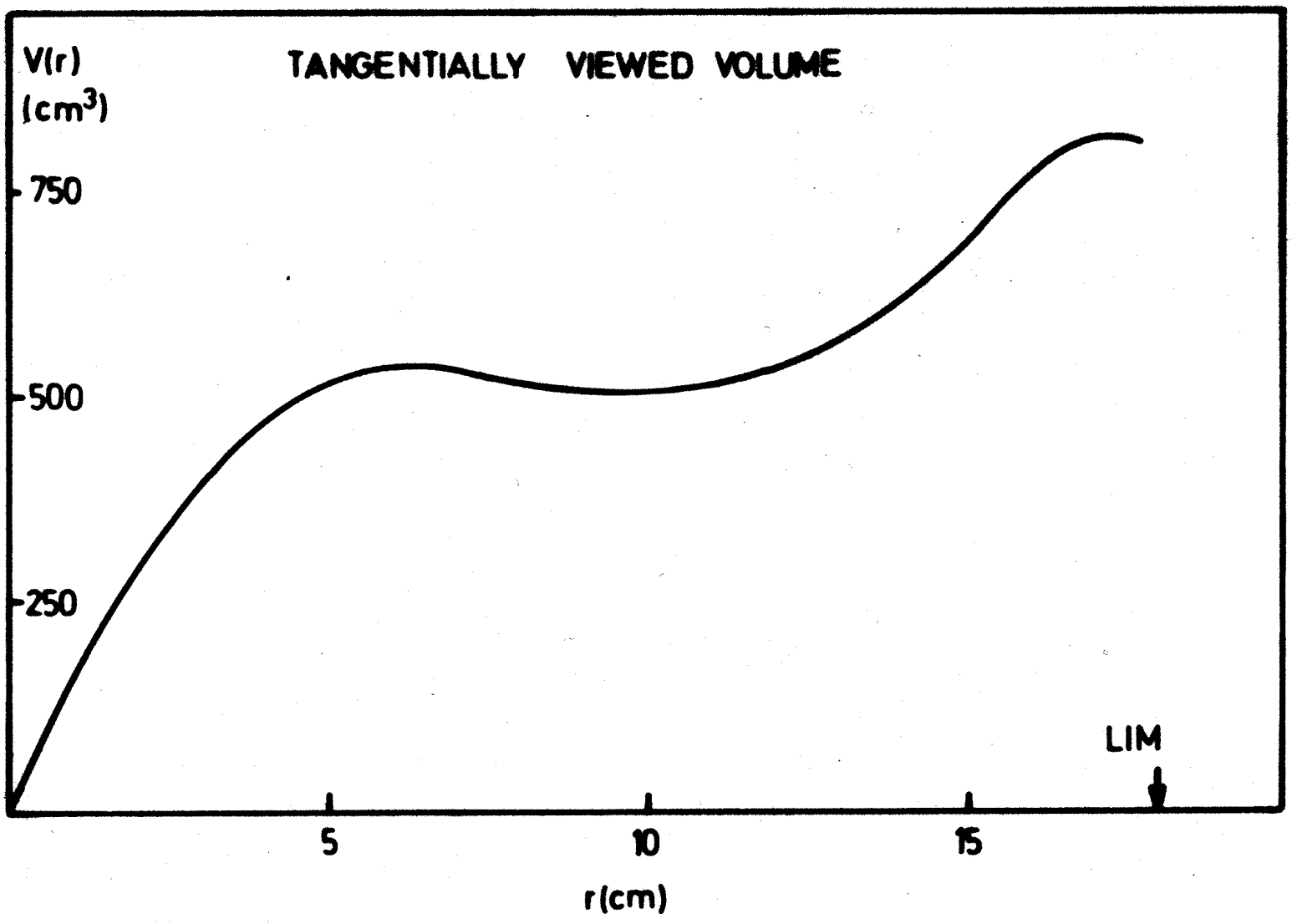

FIG. 11

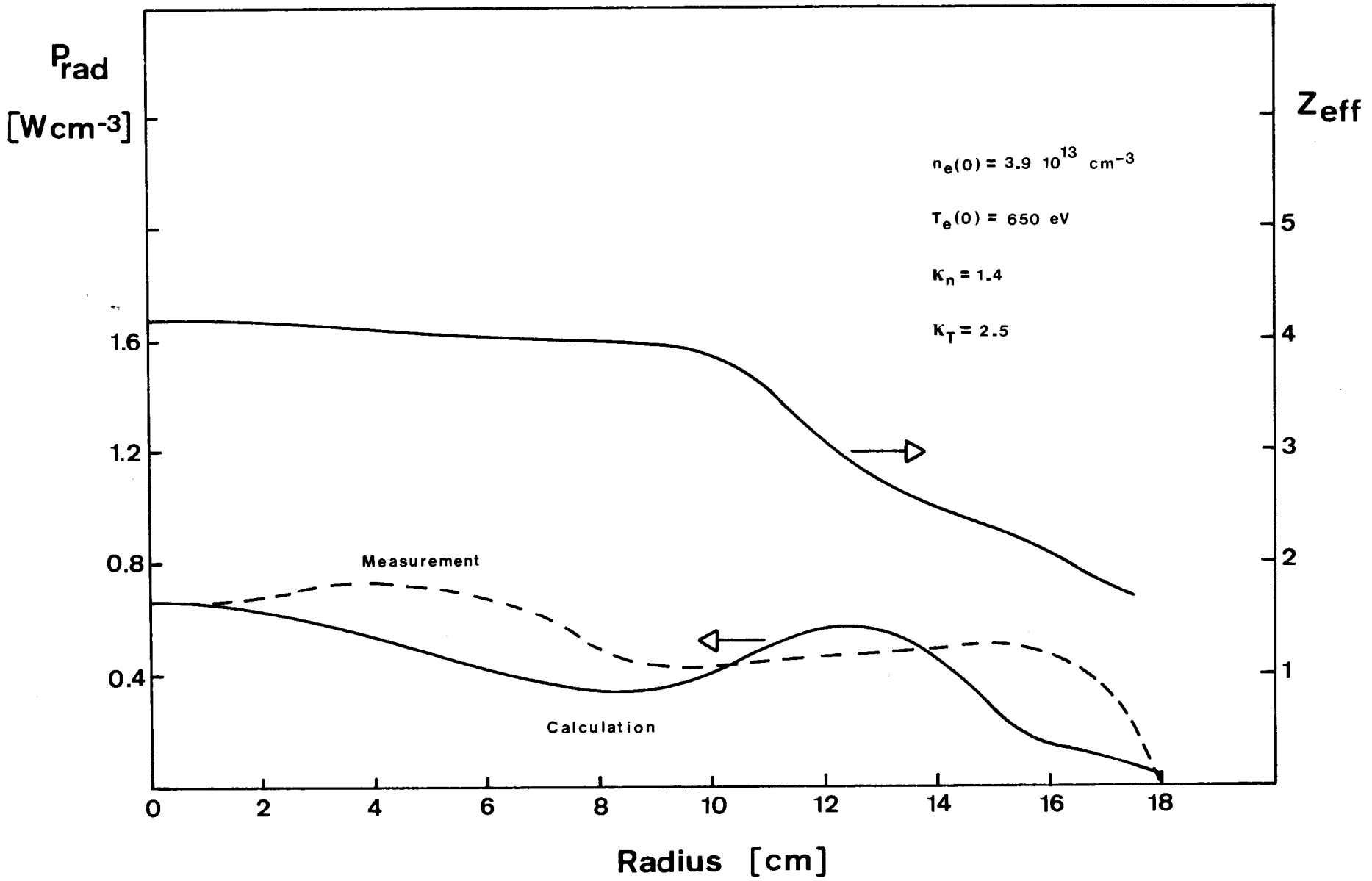
P_{rad}
[Wcm^{-3}]
Z_{eff}
$n_e(0) = 3.9\ 10^{13}\ cm^{-3}$
$T_e(0) = 650\ eV$
$K_n = 1.4$
$K_T = 2.5$
1.6
1.2
0.8
0.4
5
4
3
2
1
Measurement
Calculation
0
2
4
6
8
10
12
14
16
18
Radius [cm]

FIG. 12

FIG.1

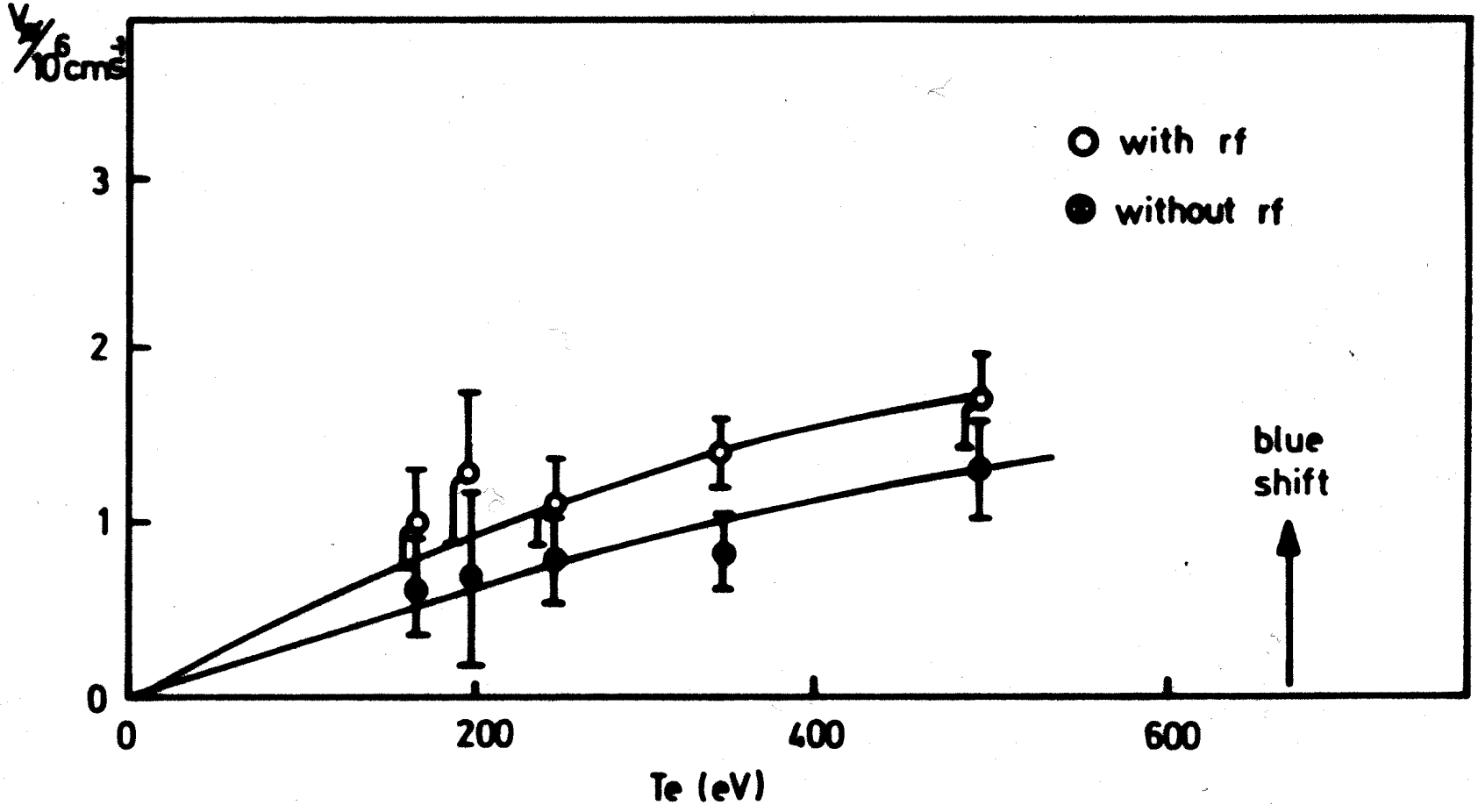

FIG. 1a Toroidal velocity